Proceedings of the Canadian Society for Mechanical Engineering International Congress 2021
CSME Congress 2021
June 27-30, 2021, Charlottetown, PE, Canada

Dynamic simulation of a roller bearing by combining finite element and lumped parameter models

Ali Safian[1], Nan Wu[1], Xihui Liang[1*]
[1]Department of Mechanical Engineering, University of Manitoba, Winnipeg, Canada
*Xihui.Liang@umantioba.ca

Abstract— Bearing dynamic modeling is an appropriate method for understanding the dynamic behavior of the bearing for different purposes such as fault diagnosis. In previous studies, the majority of researchers have focused on simulating accurate acceleration signals since accelerometer sensors are typically used for fault diagnosis in industries. Currently, there is a significant trend toward using strain sensors for the application of bearing load measurement and fault diagnosis. Recent studies have shown that measurement of strain signal is less subjected to mechanical noise compared with accelerometer sensors. Therefore, in this paper, a bearing dynamic model by combining lumped-parameter and finite element method is proposed which both accurate acceleration and stress/strain distribution can be obtained. Compared with previous combined analytical and finite element models, more accurate assumptions such as a flexible pedestal, accurate contact stress distribution, and defect geometry are included in the model which increases the accuracy of the results. In this model, a lumped-parameter model is developed for a cylindrical roller bearing in MATLAB® R2018. The contact forces of the rollers are exported into ANSYS APDL for a transient analysis. Due to considering a flexible pedestal for the bearing, a more realistic acceleration signal with a lower amplitude than the rigid model is achieved through the proposed model. Also, accurate surface/subsurface stresses are simulated due to considering contact pressures rather than concentrated forces. Overall, the proposed finite element model is a computationally efficient and accurate method for both vibration and stress/strain analysis.

Keywords-Bearing defect; finite element; condition monitoring; lumped parameter model

I. INTRODUCTION

The majority of rotating machinery includes rolling element bearings, which play a vital role in controlling the smooth rotation of the shaft. Bearings are always prone to defect due to contact and friction among their subcomponents, and it is very important to identify their defects at the incipient level. This provides enough time to take maintenance actions in the early stages to prevent fault progression and abrupt failure [1]. To have a better understanding of the bearing dynamic at a defective and non-defective level, numerous researchers have developed and modified bearing dynamic models besides their experimental studies.

Multi-body dynamic is the most common type of simulation for bearings that mass, stiffness, and damping of the bearing components are considered to create accurate interaction among them. In some cases, the components of the bearings, such as the inner/outer ring and rolling element, are modeled by rigid masses, known as lumped parameter model (LPM). Another approach is using finite element method (FEM) that the bearing dynamic can be modeled by deformable components [2]. As a few examples for bearings LPM, Sopanen and Mikkola [3] developed a bearing LPM by including various parameters including surface roughness, waviness, local fault, distributed fault, and the effect of elastohydrodynamic lubrication (EHL). Sawalhi and Randall [4] established a 34-DOF combined gear/bearing lumped parameter model in which different types of faults on the main components of the bearing were modeled, such as inner race, outer race, and rollers.

Generally, LPM is an effective method with a low computation time that analytically proves the dynamic of bearings. However, the most important output of the bearing LPM is the acceleration signal, which means that new findings and enhancements are just limited to the situation that accelerometer sensors are being used for condition monitoring. However, the major disadvantage of accelerometer sensors is that they are easily influenced and disturbed by sources of mechanical noise and they give a general signal of the system [5]. Also, due to the transmission path between the sensor and the fault, the propagated wave from the fault loses its energy to reach the sensor [6]. In the early stages of the fault, these small fault symptoms will be masked by the surrounding noise or they lose their energy due to structural damping.

To overcome this problem, several researchers have proposed the measurement of strain signal instead of acceleration. As an example, Alien et. al [7] utilized a fiber-Bragg grating (FBG) sensor to measure strain changes in a bearing test system. The results showed that not only strain signal has a better signal to noise ratio, but also it is very sensitive to the existence of a local defect. Recently, measurement of bearing strain is a trending discipline in

condition monitoring, both for fault diagnosis and overload detection [8]. However, the majority of previous works were conducted experimentally and there was not a clear understanding of strain changes on the whole bearing assembly. Therefore, having a bearing finite element (FE) model, where deformable bearing components can be modeled, will help the understanding of strain changes in bearings.

Generally speaking, bearing FE models are computationally demanding due to nonlinearity and contact among several components [9]. To overcome this difficulty, several researchers have suggested combining the analytical solution with FEM to simplify the model by removing the components in contact. As an example, Kiral and Karagulle [10] combined an analytical solution with FEM to simulate a bearing dynamic with localized fault. The outer ring and housing of the bearing were modeled by FEM, and contact forces from the analytical solution were applied to the nodes over time. For simulating the local defect, contact forces were manually increased at the defect location. In another example, Tadina and Boltezar [11] created a bearing outer ring by flexible beam elements, and the contact forces at each node were obtained through a bearing LPM. However, by using beam elements, the actual geometry of the housing/pedestal, and subsequently, realistic boundary conditions could not be simulated. Another common problem in previous studies was applying concentrated forces on the nodes. In fact, during the contact of rolling elements and raceways, a contact pressure is generated over a certain contact area, according to Hertz's contact theory [12]. This stress distribution cannot be simulated by a single nodal force, and instead, accurate area pressure on a contact area with a fine mesh must be applied.

The main purpose of this study is a combined bearing LPM and FEM with an accurate stress/strain distribution. However, the previously developed models cannot satisfy the requirement of this study due to several inaccurate assumptions. To illustrate more, a new bearing dynamic model for a cylindrical roller bearing is proposed in this study which shortcomings of previous studies are addressed. For this model, a roller bearing LPM is created in MATLAB®, and contact forces of the rollers in healthy and defective conditions are obtained over time. Contrary to reference [10] where contact forces of the defective bearing were amplified manually, the contact forces of the developed model are dependent on the geometry of the fault and accurate fluctuations of the contact stiffness. Then, the bearing LPM is combined with a FE model developed in ANSYS APDL in which actual geometries of the bearing housing, pedestal, and outer ring are modeled. This leads to applying realistic boundary conditions to the model and not over-stiffening the model by a clamped boundary condition. In contrast to previous studies, the contact forces from the bearing LPM are converted to area pressure by Hertz's contact theory. Therefore, instead of applying concentrated forces on the nodes, contact pressures are directly applied to the model which creates accurate stress distribution. In the following, the details of the proposed model are described.

II. DYNAMIC MODELING OF A ROLLER BEARING WITH A LOCAL DEFECT

A. *Lumped Parameter Model of a Roller Bearing*

In this section, a cylindrical roller bearing model SKF N305 ECP with a split pillow block housing model SKF SNL 506-605 is modeled by LPM. The 3D CAD model is illustrated in Fig 1. The diagram of the bearing LPM is also shown in Fig 2. The model includes several masses connected to each other by spring and dampers. Basically, the model is based on the given formulation in [4] with minor changes that will be described in the following. In Fig 2, subscripts x and y refer to the horizontal and vertical direction, respectively. Here, K_h, K, and K_s indicate the housing stiffness, load-deflection factor, and shaft stiffness, respectively. Parameters C_h, C_r, and C_s refer to housing damping, viscous contact damping, and shaft damping. m_{ho} includes the mass of the housing and pedestal together, and m_{si} indicates the mass of the shaft and the inner ring both together. Also, Fr is the applied vertical load from the shaft to the bearing inner ring, and φ_j illustrates the angular position of each roller over time. There are a few assumptions in the modeling of this roller bearing such as neglecting slippage, the friction of rollers, and the effect of the lubricant film. Besides, due to the moderate rotational speed of the shaft, the centrifugal force of the rolling elements and corresponding deformations are neglected. In this model, the shaft rotates at a rotational speed of ω_s. According to the bearing dimensions, such as pitch diameter D_p, roller diameter D_r, and contact angle of rollers α, the cage speed ω_c can be defined as below.

$$\omega_c = \frac{\omega_s}{2}\left(1 - \frac{D_r \cos(\alpha)}{D_p}\right) \tag{1}$$

The major role of the bearing cage is creating equal angles between rollers. Based on these equal angles and the initial position of the rollers φ_0, the angular position of rollers φ_j can be obtained for the time increment t during the rotation as below:

$$\varphi_j(t) = \frac{2\pi j}{Z} + \omega_c t + \varphi_0\,, \quad j = 1 \text{ to } z \tag{2}$$

where j and Z refer to the roller number and the total number of rollers, respectively. The applied radial force to bearing leads to radial displacement of the inner ring/shaft and the housing. Subsequently, contact deformation can be calculated by Eq. (3) which is dependent on the radial clearance of the bearing C, the angular position of each roller, and in case of having a local defect, the depth of the fault C_d. The term β_j is switch function and is equal to 1 when a roller enters the defective area, and it is zero for rollers in the healthy areas. In Eq. (4), φ_d indicates

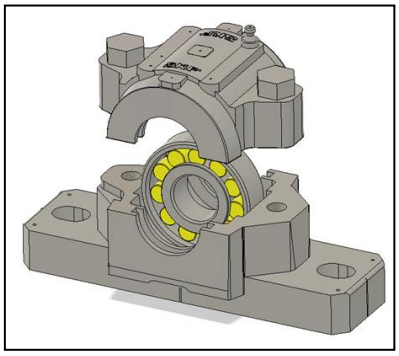

Figure 1. 3D CAD assembly of the bearing and split pillow housing.

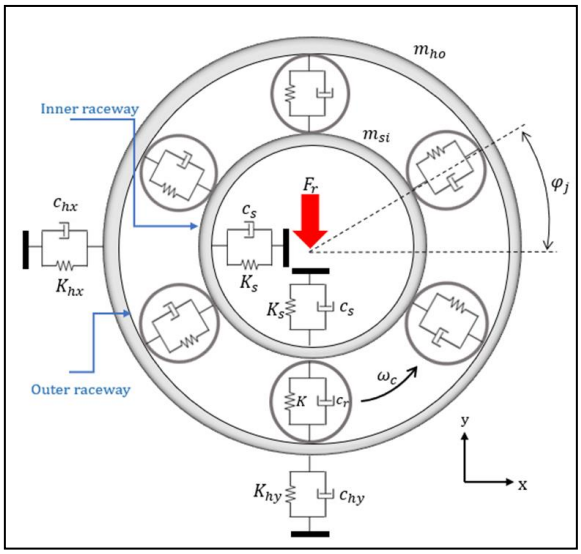

Figure 2. Diagram of the roller bearing LPM.

the starting angular position of the defect and $\Delta\varphi_d$ refers to the angular distance that is covered by the local defect.

$$\delta_j = (X_{si} - X_{ho})\cos\varphi_j + (Y_{si} - Y_{ho})\sin\varphi_j - C - \beta_j C_d \quad (3)$$

$$\beta_j = \begin{cases} 1 & \text{if} \quad \varphi_d < \varphi_j < \Delta\varphi_d + \varphi_d \\ 0 & \text{otherwise} \end{cases} \quad (4)$$

Based on the defined equations and parameters, a 4-DOF non-linear equation of motion is presented as below:

$$m_{si}\ddot{X}_{si} + C_s\dot{X}_{si} + K_sX_{si} + \sum_{j=1}^{Z}\alpha_j C_r\dot{\delta}_j\cos\varphi_j + \sum_{j=1}^{Z}\alpha_j K(\delta_j)^n\cos\varphi_j = 0 \quad (5)$$

$$m_{si}\ddot{Y}_{si} + C_s\dot{Y}_{si} + K_sY_{si} + \sum_{j=1}^{Z}\alpha_j C_r\dot{\delta}_j\sin\varphi_j + \sum_{j=1}^{Z}\alpha_j K(\delta_j)^n\sin\varphi_j = -F_r \quad (6)$$

$$m_{ho}\ddot{X}_{ho} + C_{hx}\dot{X}_{ho} + K_{hx}X_{ho} - \sum_{j=1}^{Z}\alpha_j C_r\dot{\delta}_j\cos\varphi_j - \sum_{j=1}^{Z}\alpha_j K(\delta_j)^n\cos\varphi_j = 0 \quad (7)$$

$$m_{ho}\ddot{Y}_{ho} + C_{hy}\dot{Y}_{ho} + K_{hy}Y_{ho} - \sum_{j=1}^{Z}\alpha_j C_r\dot{\delta}_j\sin\varphi_j - \sum_{j=1}^{Z}\alpha_j K(\delta_j)^n\sin\varphi_j = 0 \quad (8)$$

According to Hertz's contact theory, for a cylindrical roller bearing (line contact), the exponent n is equal to 10/9. The term α_j refers to the bearing load zone parameter which is equal to zero once δ_j is equal/less than zero which means the roller is not positioned in the load zone of the bearing and its contact forces will not be considered. Once the roller enters the load zone, δ_j will be greater than zero and α_j will be equal to 1 in order to include its contact forces. α_j is defined as below [12]:

$$\alpha_j = \begin{cases} 1 & \text{if} \quad \delta_j > 0 \\ 0 & \text{if} \quad \delta_j \le 0 \end{cases} \quad (9)$$

The contact forces in the horizontal and vertical direction can be calculated as follows:

$$\begin{bmatrix} F_x \\ F_y \end{bmatrix} = \begin{bmatrix} \sum_{j=1}^{Z}\alpha_j C_r\dot{\delta}_j\cos\varphi_j + \sum_{j=1}^{Z}\alpha_j K(\delta_j)^n\cos\varphi_j \\ \sum_{j=1}^{Z}\alpha_j C_r\dot{\delta}_j\sin\varphi_j + \sum_{j=1}^{Z}\alpha_j K(\delta_j)^n\sin\varphi_j \end{bmatrix} \quad (10)$$

The load-deflection factor K is the summation of contact stiffness of a roller with the inner raceway and outer raceway as shown in Eq. (11). For each raceway, the contact stiffness $K_{in/out}$ is obtained by Eq. (12) [12].

$$K = \left[\frac{1}{\left(\frac{1}{K_{in}}\right)^{\frac{1}{n}} + \left(\frac{1}{K_{out}}\right)^{\frac{1}{n}}}\right]^n \quad (11)$$

$$K_{in/out} = \frac{l_e^{\frac{8}{9}}}{0.39^{\frac{10}{9}}\left[\frac{4(1-\upsilon_1^2)}{E_1} + \frac{4(1-\upsilon_2^2)}{E_2}\right]} \quad (12)$$

where l_e refers to the effective length of the line contact, υ is the Poisson's ratio, E is Young's modulus, and subscripts 1 and 2 indicate two different material properties. The model parameters of the bearing LPM are estimated by FEM and their values with other constant parameters in this modeling are presented in Table I.

Despite using bearing LPM, for a defect-free roller bearing with certain clearance, the radial contact forces for different positions of the rollers can be properly estimated by the Stribeck formula as follows [12]:

$$Q_{jr} = Q_{max}\left[1 - \frac{1-\cos(\varphi_j)}{2\epsilon}\right] \quad (13)$$

where Q_{max} is the maximum radial load applied to a roller, and load distribution factor ϵ is equal to 0.5 for zero clearance, for positive clearance in the range of $0 < \epsilon < 0.5$, and for negative clearance $0.5 < \epsilon < 1$. By using Eq. (13), the accuracy of the contact forces from the developed LPM can be validated in a healthy condition. Also, the maximum value of the contact forces (Q_{max}) for zero clearance can be calculated as follows [12]:

$$Q_{max} = \frac{4.08\,F_r}{Z\cos(\alpha)} \quad (14)$$

The dynamic model of this cylindrical bearing is modeled in MATLAB® based on the aforementioned equations and constant parameters in Table 1. By using ordinary differential equations solver (ODE45) which is based on the Runga-Kutta method, the equations of motion (5) to (8) have been solved. A vertical displacement of 1×10^{-6} m is considered for the shaft as the initial condition which has a rotational speed of 1000 rpm. Moreover, contact forces in the vertical and horizontal directions are calculated according to Eq. (10) in two separate matrices that rows represent the number of rollers through 1 to 11, and each column refers to the value of contact forces in each time increment.

B. Description of the Proposed Finite Element Model

According to the Hertz contact theory, the area generated and contact pressure distribution of ball bearings and cylindrical rollers bearing can be calculated. In deep groove ball bearings, the contact area has an elliptical shape and for cylindrical roller bearings, the generated area is similar to a narrow rectangular band as shown in Fig. 3. The width of the contact is shown by 2a and l_e indicates the length of the rectangular band. Half of the contact width and the contact pressure are calculated by Eqs. (15) and (16), respectively [12].

TABLE I. ESTIMATED MODEL PARAMETERS OF THE BEARING LPM.

Model Parameter	Details of Model Parameters		
	Sign	*Value*	*unit*
Roller diameter	D_r	10	mm
Effective length of contact	l_e	10.2	mm
Bearing pitch diameter	D_p	44	mm
Bearing outer raceway diameter	D_{out}	54	mm
Number of rollers	Z	11	-
Bearing clearance	ϵ	0	-
Load deflection factor	K	618.02	$MN/m^{1.11}$
Viscous contact damping	C_b	3800	N.s/m
Housing vertical stiffness	K_{hy}	88.9	MN/m
Housing horizontal stiffness	K_{hx}	412.1	MN/m
Housing vertical damping	C_{hy}	600	N.s/m
Housing horizontal damping	C_{hx}	2110	N.s/m
Mass of the housing and outer ring	m_{ho}	18.165	Kg
Shaft stiffness	K_s	0.201	MN/m
Shaft damping	C_s	380	N.s/m
Mass of the shaft and inner ring	m_{si}	3.8	Kg
Young's modulus of the components	E	200	GPa
Poisson's ratio of the components	υ	0.3	-
Defect depth	C_d	0.2	mm

$$a = \sqrt{\frac{4F\left[\frac{1-\upsilon_1^2}{E_1} + \frac{1-\upsilon_2^2}{E_2}\right]}{\pi l_e\left(\frac{1}{R_1} - \frac{1}{R_2}\right)}} \tag{15}$$

$$P = \frac{2F}{\pi a l_e}\left(1 - \frac{x^2}{a^2}\right)^{\frac{1}{2}} \tag{16}$$

where F refers to the radial load applied on a roller, R_1 and R_2 indicate the radius of the roller and outer raceway, respectively. By substituting x=0 in Eq. (16), the maximum contact pressure is calculated.

The geometry of the proposed bearing FEM is dependent on the housing dimension, outer/inner ring diameter, and the contact width in Eq. (15). Since rollers are only under radial forces, and it is assumed that the cross-section is constant in the normal direction, this FEM can be modeled as plane strain with 2D elements with neglecting normal strain changes.

The matrix of contact forces obtained from Eq. (10) is converted into equivalent normal forces to the raceway because the matrix represents forces in x and y directions. Also, by substituting the equivalent contact forces into Eq (15), the contact width of each roller is obtained over time.

By considering zero clearance for the bearing, it is observed that the load zone of the bearing is at the bottom half of the outer raceway and there is not any contact with the upper section. Therefore, the bottom half of the FE model is considered for applying contact forces. The raceway is divided into equally spaced contact points, and for each point, a line proportional to the contact width by Eq. (15) is considered. These small lines are named contact lines in this paper. Obviously, by having a higher number of contact points, the number of contact lines will be increased, and meanwhile, the sampling frequency of the model is increased. After creating the geometry of the outer ring, other parts of the bearing and housing geometry are created by simple straight lines and arcs. The outer ring, housing, and pedestal are glued to each other at the contact location. Also, Equivalent radial forces are changed to contact pressures over time by Eq. (16) and finally, they are applied to contact lines. By using fine mesh on the outer raceway, and gradually increasing the element size to the outer ring surface, the meshing process is done, and a transient analysis can be started. The meshed geometry with a magnified view of the local defect is illustrated in Fig. 4.

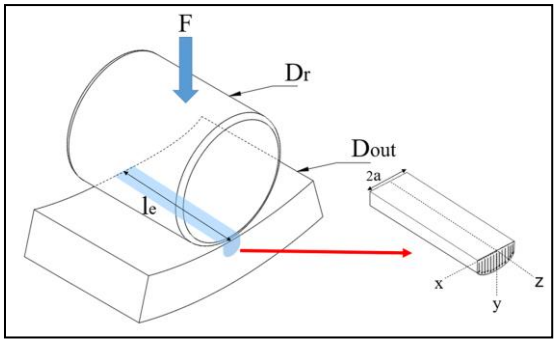

Figure 3. Contact width and pressure distribution of a roller during contact

III. COMPARISON OF NORMAL STRESS DISTRIBUTION

In this section, prior to analyzing the dynamic response of the model, the accuracy of the stress distribution is investigated. For this comparison, a static analysis including the proposed FE model and a 3D contact model is performed. A radial load (F_r) of 500 N is considered for the model. By substituting this value in Eq. (14), the maximum value of contact force is equal to 185.45 N. Similarly, the maximum contact force obtained from the bearing LPM is equal to 184.4 N. This 0.56% difference indicates the accuracy of the developed bearing LPM in generating contact forces of the rollers. By using Hertz's theory and substituting the maximum contact force in Eqs. (15) and (16), half of the contact width and the maximum contact pressure are equal to 0.036 mm and 321 MPa, respectively. For comparison of the stress distribution, a bearing 3D model is created in ANSYS as shown in Fig. 5. Since the geometry of this model is symmetric in the YZ plane, a symmetric boundary condition is applied to the YZ plane (Ux=0). Also, the axial displacement of the components in the z-direction is constrained. These boundary conditions reduce the computation time and rigid body motion as well. Due to considering symmetric boundary condition in the YZ plane, half of the maximum contact force is applied to

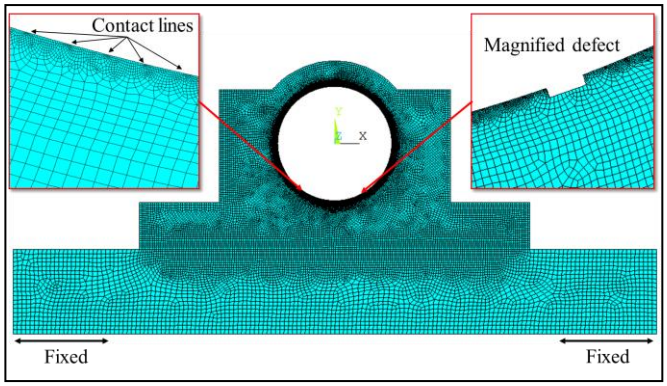

Figure 4. The meshing of the bearing assembly in ANSYS APDL with a magnified view of the defect.

the roller upper surface (92.73 N). Since Hertz's theory is based on frictionless contact [12], a frictionless contact is applied between the roller and outer ring. By applying fine mesh at the contact location and solving the model, the normal stress distribution and the contact pressure are obtained on the outer ring. Besides, the contact pressure of 321 MPa is applied to the corresponding contact line in the proposed bearing FE model in a static analysis. The generated stress distribution of the proposed FE model and 3D contact model is compared in Fig. 6. It must be cautioned that due to applying load on the roller in -y-direction, the minimum value of stress with a negative sign indicates the maximum generated stress.

Comparing the contact stress in the 3D FE model vs the value obtained by Hertz's theory (321 MPa) reveals that the created 3D model generates the same contact stress as Hertz's theory. In Fig. 6, the maximum contact stress of the 3D model is equal to 320.45 MPa and the difference with Hertz's theory is about 0.45%. However, the maximum stress of the proposed FE model is about 15% higher than the theoretical value (321 MPa). Since in the proposed FE model, uniform pressure is applied to the contact line, two stress concentrations happen at the starting and ending point of the contact line, which increases the maximum generated stress. This stress concentration is shown by "Max" in Fig. 6. Nevertheless, the average stress on the nodes of the contact line is equal to 329.33 MPa and the estimated error compared with Hertz's theory is 2.92%. Therefore, comparatively accurate contact stress has been simulated through the proposed FE model. Last but not least, the subsurface stress of the proposed FE model and the 3D model can be investigated in Fig. 6. Obviously, the stress bulb in the proposed FE model is comparatively similar to the 3D model, and it can be concluded that the proposed FE model is accurate both in creating surface and subsurface stresses.

IV. Results and Discussion

After comparing the stress distribution in the proposed model, the dynamic behavior of the proposed FE model is investigated through a transient analysis in this section.

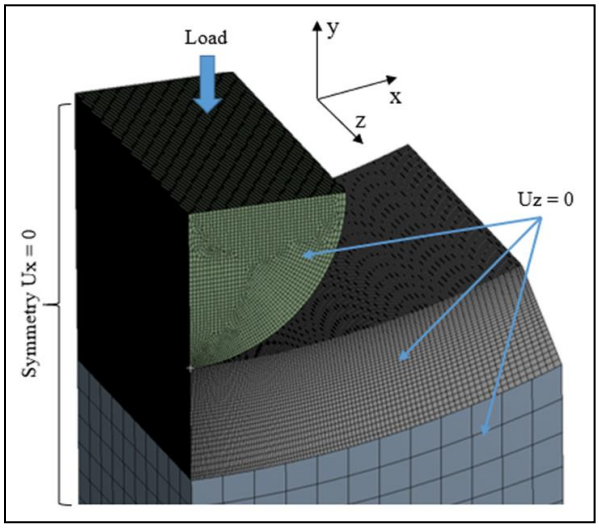

Figure 5. 3D FE model of the roller in contact with the outer ring.

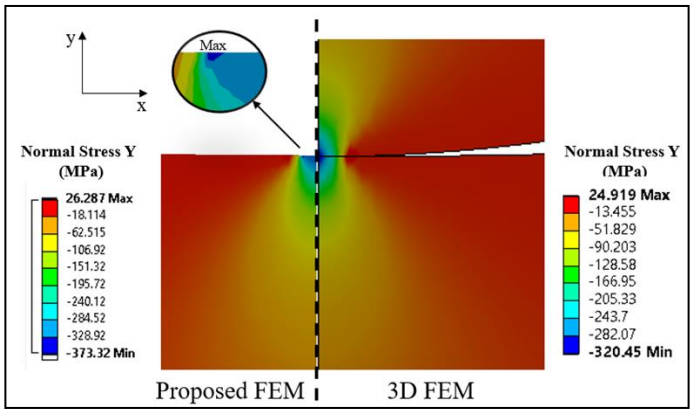

Figure 6. Stress distribution of the 3D contact model vs proposed FEM.

The geometry of the housing and outer ring was shown in Fig. 4. The rotational speed of the shaft is 1000 rpm, and the radial applied load is equal to 500 N. The ball pass frequency on the outer ring (BPFO) can be calculated as follows [12]:

$$\mathrm{BPFO} = \frac{z}{2}\,\omega_s\left(1 - \frac{D_r}{D_p}\right) \tag{17}$$

Therefore, for the shaft speed of 1000 rpm, the BPFO is equal to 70.8 Hz. In order to accurately capture the roller entry and exit on the fault, a higher sampling frequency than the BPFO is considered in this model. As an example, by considering a sampling frequency 36 times higher than the BPFO, a sampling frequency around 2500 Hz is obtained for the transient analysis. This means the outer ring has to be divided into 11×36 = 396 contact locations where 11 refers to the number of rollers. Therefore, by dividing the outer ring into 396 contact locations (contact lines), the angular distance between each two contact locations is 0.01586 rad. By considering a rotational speed of 1000 rpm (104.71 rad/s), the time increment from one contact location to the next one is equal to 0.000392156 s. Hence, the sampling frequency of the simulation is equal to 1/0.000392156 ≈ 2550 Hz. The time-step of the LPM can be much smaller than the FEM since it does not require a large computation time. The time step of the bearing LPM is selected to be 300 times lower than the FE model, which is equal to 1.307×10^{-6} s. After running the bearing LPM, time-dependent contact pressures are sampled every 300 steps to be used as the input of the transient analysis. By running the simulation for a defective bearing, the time domain acceleration signals of the proposed FE model and LPM are shown in Fig. 7. The local defect is located at 289° (φ_d), has a 0.19 mm depth (Cd), and 1.8° spall width ($\Delta\varphi_d$). According to Fig. 7, the amplitude of the acceleration signal is modulated by several resonances due to the impact between rollers and the local fault.

The time interval between resonant peaks of the raw vibration signal is equal to 1/70.8 ≈ 0.0141 s, which are accurately shown in Fig. 7. The amplitude range of the acceleration signal from the proposed FE model is lower than the LPM. This difference is one advantage of the proposed model where a flexible pedestal is modeled for the bearing. Also, the envelope spectrum of the acceleration signal is shown in Fig. 8 in the frequency domain. The BPFO (around 70.8 Hz) and its harmonics are accurately shown in the frequency-

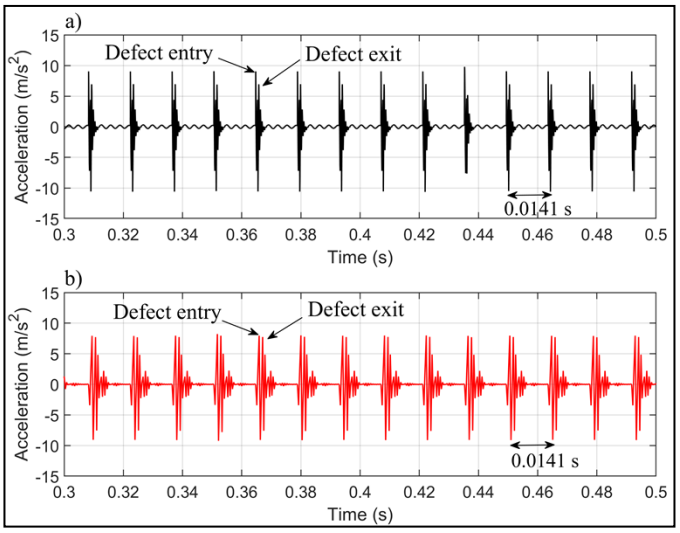

Figure 7. Simulated acceleration by a) bearing LPM b) proposed FEM.

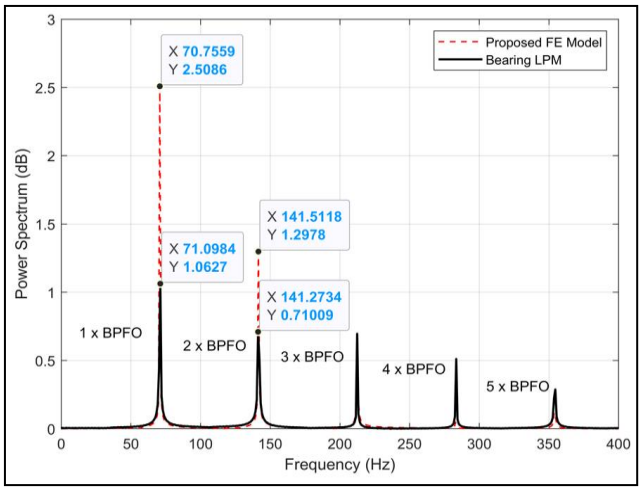

Figure 8. Envelope spectrum of the acceleration signal from the bearing LPM and the proposed FE model.

domain which shows the efficiency of the proposed FE model in generating vibration signal and frequency components of the system. Overall, the proposed model is an efficient option for the dynamic analysis of roller bearings, especially, if the focus is simulating dynamic stress/strain changes. Through the proposed FE model, stress distribution and strain signal can be obtained by a reasonable computation time. For future work, a thin layer of a piezoelectric patch will be glued on the bearing outer ring surface to measure the strain changes. The measured strain signal will be compared with the simulated strain signal through the proposed FE model. This technique will be used for fault diagnosis in bearings through strain signals.

Conclusion

In this paper, a combined bearing LPM and FE model was proposed to simulate the dynamic behavior of a roller bearing with a local fault. Contrary to previous combined analytical and FE models that the main purpose was simulating acceleration signal, this study focuses on generating both accurate acceleration and stress/strain distribution. At the first stage, a 4-DOF bearing LPM was created in MATLAB® and solved with an ordinary differential equations solver (ODE45). The contact forces were converted to contact pressures by Hertz's contact theory to be exported to the FE model. In the second stage, a flexible bearing assembly was modeled in ANSYS APDL and time-dependent contact pressures were applied to the bearing outer ring through transient analysis. The accuracy of the stress distribution was investigated in a static model, and the result agreed with Hertz's theory and a 3D FE model. After this validation, the dynamic response of the proposed model was investigated. A reasonable acceleration signal in the time and frequency domain was simulated through the proposed FE model which accurately demonstrates the fault symptoms. In this paper, due to considering flexible components, the acceleration signal had a lower amplitude than the LPM model, since LPM is based on the interaction of rigid components. For future work, this model will be used for the application of embedded strain sensors for fault diagnosis.

References

[1] W. Mao, S. Tian, J. Fan, X. Liang, and A. Safian, "Online detection of bearing incipient fault with semi-supervised architecture and deep feature representation," *J. Manuf. Syst.*, vol. 55, pp. 179–198, Apr. 2020.

[2] D. Petersen, C. Howard, N. Sawalhi, A. Moazen Ahmadi, and S. Singh, "Analysis of bearing stiffness variations, contact forces and vibrations in radially loaded double row rolling element bearings with raceway defects," *Mech. Syst. Signal Process.*, vol. 50–51, pp. 139–160, Jan. 2015.

[3] J. Sopanen and A. Mikkola, "Dynamic model of a deep-groove ball bearing including localized and distributed defects. Part 2: Implementation and results," *Proc. Inst. Mech. Eng. Part K J. Multi-Body Dyn.*, vol. 217, no. 3, pp. 213–223, Sep. 2003.

[4] N. Sawalhi and R. B. Randall, "Simulating gear and bearing interactions in the presence of faults," *Mech. Syst. Signal Process.*, vol. 22, no. 8, pp. 1924–1951, Nov. 2008.

[5] Y. Qu, H. Zhang, L. Hong, C. Zhao, Y. Tan, and Z. Zhou, "On research of incipient gear pitting fault detection using optic fiber sensors," in *2018 IEEE International Instrumentation and Measurement Technology Conference (I2MTC)*, May 2018, pp. 1–6.

[6] X. Liang, M. J. Zuo, and Z. Feng, "Dynamic modeling of gearbox faults: A review," *Mech. Syst. Signal Process.*, vol. 98, pp. 852–876, Jan. 2018.

[7] H. Alian, S. Konforty, U. Ben-Simon, R. Klein, M. Tur, and J. Bortman, "Bearing fault detection and fault size estimation using fiber-optic sensors," *Mech. Syst. Signal Process.*, vol. 120, pp. 392–407, Apr. 2019.

[8] A. Reid *et al.*, "Measurement of strain evolution in overloaded roller bearings using energy dispersive X-ray diffraction," *Tribol. Int.*, vol. 140, p. 105893, Dec. 2019.

[9] C. Machado, M. Guessasma, and E. Bellenger, "An improved 2D modeling of bearing based on DEM for predicting mechanical stresses in dynamic," *Mech. Mach. Theory*, vol. 113, pp. 53–66, Jul. 2017.

[10] Z. Kiral and H. Karagülle, "Simulation and analysis of vibration signals generated by rolling element bearing with defects," *Tribol. Int.*, vol. 36, no. 9, pp. 667–678, Sep. 2003.

[11] M. Tadina and M. Boltežar, "Improved model of a ball bearing for the simulation of vibration signals due to faults during run-up," *J. Sound Vib.*, vol. 330, no. 17, pp. 4287–4301, Aug. 2011.

[12] T. A. Harris, *Rolling bearing analysis*, 4th ed. New York: Wiley, 2001.